Delivery and expression of mRNA therapeutics during ex vivo kidney perfusion: A feasibility study in porcine and human donor kidneys

Cristina Ballester[1,2†], Ping Song[3†], Katerina B Knudsen[1,2], Chris Jaynes[4,5], Henri Leuvenink[4,5], Victor R Llorente[1,2], Annick Van Furth[4], Rikke Nørregaard[1], Jan-Luuk Hillebrands[6], Anna Krarup Keller[1,7], Bente Jespersen[1,2], Jørgen Kjems[3#], Marco Eijken[1,2#]

[1]Department of Clinical Medicine, Aarhus University, Aarhus, Denmark

[2]Department of Renal Medicine, Aarhus University Hospital, Aarhus, Denmark

[3]Interdisciplinary Nanoscience Center (iNANO), Aarhus University, Aarhus, Denmark

[4]Department of Surgery, University Medical Center Groningen, Groningen, The Netherlands

[5]34Lives, Public Benefit Company, West-Lafayette, Indiana, United States

[6]Department of Pathology, University Medical Center Groningen, Groningen, The Netherlands

[7]Department of Urology, Aarhus University Hospital, Aarhus, Denmark

[†] Shared first authors

[#] Shared last authors

Corresponding author: Cristina Ballester Bergada. Department of Clinical Medicine-Renal Medicine, Aarhus University, Aarhus, Denmark. Addressee: Palle Juul-Jensens Blvd. 82, 8200 Aarhus, Denmark address. Mail: crisballester@clin.au.dk.

Running title: mRNA delivery during donor kidney perfusion

ABSTRACT

Ischemia–reperfusion injury (IRI) is a major cause of graft dysfunction in donor kidneys. Normothermic machine perfusion (NMP) offers a clinically relevant ex vivo platform for targeted intervention during organ preservation, while minimizing systemic exposure. Here, we investigated lipid nanoparticle (LNP)-mediated mRNA delivery during NMP as a strategy to enable immediate post-transplant therapeutic activity. Porcine and human kidneys were perfused at 37 °C for 6–12 h with an erythrocyte-based perfusate, and LNP-encapsulated mCherry or human erythropoietin (hEPO) mRNA was administered via the renal artery. Intravascular LNP delivery resulted in widespread renal parenchymal uptake of reporter mRNA without evidence of vascular obstruction or histological injury. hEPO protein became detectable in the perfusate approximately 2 h after infusion and continued to increase throughout perfusion, reaching biologically relevant concentrations. LNPs incorporating PEG-lipid TPGS (D-α-tocopherol polyethylene glycol 1000 succinate) achieved significantly higher mRNA delivery efficiency than conventional DSPE-PEG2000 formulations. The findings provide a foundation for the use of LNPs and mRNA therapeutics during organ machine perfusion as a platform for precision medicine in the field of kidney transplantation.

45 **INTRODUCTION**

46 Recent advancements in mRNA-based therapeutics have significantly expanded their
47 potential applications in healthcare. In the field of infectious diseases, the application of
48 SARS-CoV-2 mRNA-based vaccines has been effective(1, 2). Additionally, mRNA cancer
49 vaccines have shown promising results for melanoma treatment(3). Beyond vaccines for
50 infectious diseases and cancer, synthetic mRNAs are currently being developed to encode
51 for therapeutic protein replacement therapies, immunotherapies, genome editing and
52 tissue repair(4). Numerous clinical trials exploring mRNA therapeutics are ongoing across
53 a wide range of diseases, including cystic fibrosis transmembrane conductance regulator
54 (CFTR) mRNA for cystic fibrosis and vascular endothelial growth factor A (VEGF-A) mRNA
55 for myocardial infarction(5, 6), reflecting the growing versatility and therapeutic potential
56 of this platform. Delivery of therapeutic mRNAs requires safe, effective and stable delivery
57 systems to avoid nucleic acid degradation and overcome biological barriers. Lipid
58 nanoparticles (LNPs) have been used as an efficient delivery platform to enhance mRNA
59 stability and cellular uptake(7, 8). Developing mRNA therapies for non-vaccine
60 applications presents unique challenges. Unlike vaccines, therapeutic mRNAs typically
61 require higher dosing, alternative routes of administration beyond intramuscular
62 injections, and formulation strategies for enhanced targeted delivery and functional
63 expression. In the bloodstream, certain LNPs can bind to apolipoprotein E (APOE), which,
64 in turn, interacts with the abundant low-density lipoprotein receptors (LDLRs) in the liver.
65 This interaction promotes the preferential uptake of LNPs by the liver, thereby limiting the
66 distribution of mRNA to other tissues(9). *Ex vivo* organ machine perfusion, a technique that

67 circulates a nutrient and oxygen-rich preservation solution or immune cell-depleted blood
68 substitute through the organ's vascular network to maintain its function and viability, is
69 increasingly adopted in clinical practice(10-12). The perfusion can be performed under
70 hypothermic conditions (typically 4-10°C), which minimizes metabolic activity to reduce
71 cellular damage, or under normothermic conditions (35–37°C), closely mimicking
72 physiological conditions and metabolic rates. This dynamic organ preservation technique
73 offers a unique opportunity for *ex vivo* delivery of mRNA therapeutics. It enables precise
74 tissue targeting with minimal off-target effects while achieving coverage of a whole organ,
75 which remains a critical barrier in the mRNA field. Organ machine perfusion is promising
76 for direct mRNA delivery to organs, potentially eliminating the need for complex LNP
77 modifications with targeting ligands. This approach allows for localized delivery, enabling
78 lower doses with improved safety, efficiency and cost-effectiveness. In particular,
79 normothermic machine perfusion (NMP) supports active metabolism, which can facilitate
80 LNP uptake and initiate mRNA translation prior to transplantation of the organ. We
81 hypothesize that mRNAs encoding for therapeutic proteins, delivered during NMP, present
82 a promising strategy to protect donor kidneys against ischemia-reperfusion injury (IRI). By
83 reducing the pathological reactivity of the graft triggered upon transplantation into the
84 recipient, this approach may help reduce fibrosis development, which can eventually
85 compromise graft function and survival(13). Therefore, the aim of this study is to evaluate
86 the potential of LNP-based delivery of therapeutic mRNAs to donor kidneys during *ex vivo*
87 NMP using model mRNAs as proof-of-concept.
88

RESULTS

Preparation and characterization of LNPs

In the present study, we developed three LNP formulations based on our in-house synthesized ionizable lipid, C14120, using different coating materials: PEG-lipid TPGS (TPGS-LNP), PEG-lipid DSPE-PEG2000 (DSPE-LNP), and a PEG-based block copolymer (F127-LNP). The LNPs ranged between 150 nm to approximately 175 nm in diameter and exhibited a positive surface charge with zeta potential over 30 mV and generally low polydispersity (<0.2) (Figure 1a-c). LNPs were loaded with mRNA through electrostatic interactions between ionizable lipids within the formulations and negatively charged mRNAs. mRNA encoding mCherry protein was encapsulated within the three LNP formulations at N/P ratios of 6, 12, and 16. The optimal N/P ratio for mRNA delivery and protein expression was evaluated across the three LNP formulations in OK cells. For F127-LNP and DSPE-LNP, transfection efficiency increased with higher N/P ratios, achieving maximal mCherry expression at N/P ratio of 12 and 16 respectively (Figure1d). In contrast, TPGS-LNP exhibited consistently high mCherry expression across all tested N/P ratios. Importantly, no apparent cytotoxicity was observed after 24 hours of incubation with any of the three LNP formulations at these N/P ratios (Figure 1e). Based on the balance of efficacy and safety, an N/P ratio of 12 was selected for all subsequent experiments. At this ratio, all three LNP types showed high mRNA encapsulation efficiency ranging from 80 to 90% (Figure 1f).

To assess the stability of the encapsulated mRNA, LNPs-encapsulated mCherry mRNA and free (naked) mCherry mRNA were incubated in the kidney perfusion solution (RBC-

111 free) at 37°C for up to 24 hours, with samples collected at multiple time points. The
112 remaining mCherry mRNA levels were quantified by RT-qPCR. Free mRNA exhibited rapid
113 degradation, with a sharp decline in detectable levels within the first hour of incubation. In
114 comparison, mRNA encapsulated within all three LNP formulations remained stable over
115 24 hours (Figure 1g).
116 The transfection efficiency of F127-, TPGS- and DSPE-LNP for mRNA delivery was assessed
117 in OK cells, using Cy5-labeled mRNA encoding EGFP (Cy5-EGFP). Both mRNA uptake (Cy5
118 signal) and protein expression (EGFP signal) were quantified using flow cytometry. No
119 significant difference in uptake was observed among the three formulations at 4 hours,
120 while DSPE-LNP exhibited the highest cellular uptake after 24 hours (Figure 2a,b).
121 Regarding mRNA-mediated protein expression, F127-LNP exhibited rapid EGFP expression
122 at 4 hours, whereas TPGS-LNP demonstrated the highest EGFP levels at 24 hours (Figure 2
123 a,c).
124 To further analyze protein expression efficiency, mRNAs encoding for mCherry and the
125 secreted protein, human erythropoietin (hEPO) were transfected in HKC-8 and OK cells
126 (supplemental figure 1). Similar trends were observed using both flow cytometry and ELISA
127 with these alternative reporter proteins, with TPGS-LNP consistently emerging as the most
128 efficient candidate showing a comparable pattern.
129
130 **hEPO mRNA delivery during kidney-NMP**
131 To evaluate mRNA delivery and translation during NMP, human erythropoietin (hEPO)
132 encoding mRNA was chosen as a reporter, enabling direct measurement of secreted hEPO

133 in both the perfusate and urine. Porcine kidneys (n=3-4 per treatment) were connected to
134 an NMP setup and 150 µg of DSPE or TPGS encapsulated hEPO mRNA (DSPE-hEPO and
135 TPGS-hEPO, respectively) was infused via the renal artery. The contralateral kidneys (n=6)
136 served as non-mRNA treated controls. After LNP-mRNA infusion, kidneys remained on
137 NMP for an additional six hours for follow-up. hEPO was measured in the perfusate as early
138 as two hours following mRNA administration, with levels gradually increasing to about 4
139 mIU/mL for DSPE-hEPO after 6 hours. TPGS-hEPO treated kidneys showed significantly
140 higher hEPO levels with up to 360 mIU/mL after 6 hours (Figure 3a). hEPO was also
141 detected in the urine reaching up to 6 mIU/mL and 420 mIU/mL for DSPE-hEPO and TPGS-
142 hEPO, respectively, 4-6 hours after administration (Figure 3b).
143 Perfusion characteristics, including renal blood flow, oxygen consumption and urine
144 production, were similar between porcine kidneys infused with DSPE-hEPO, TPGS-hEPO
145 and non-treated controls (Supplemental Figure 4). Hematoxylin and eosin (H&E) as well as
146 periodic acid-schiff (PAS) staining of the tissue sections showed no signs of LNP-induced
147 structural damage (Supplemental Figure 5).
148
149 **mCherry mRNA delivery during kidney-NMP**
150 To asses the possibility for localized expression of an intracellular protein, mRNA encoding
151 mCherry was administered to porcine kidneys using both DSPE- and TPGS-LNP, following
152 the same protocol as in the hEPO studies.
153 In tissue biopsies taken hourly up to 9 hours of NMP and analyzed by western blotting,
154 mCherry protein expression became apparent after 4-5 hours for TPGS-LNP and 7-8 hours

155 for DSPE-LNP, both increasing towards the end of the perfusion (9 hours; Figure 4a, b).
156 Similar to hEPO expression, TPGS-LNP exhibited greater efficacy than DSPE-LNP (Figure
157 4a, b). Analysis of cortical tissue collected from different kidney poles and the medulla
158 confirmed that the delivered mRNA reached all regions within the organ. However,
159 substantial variation in mCherry levels was observed between the tested kidneys.
160 Notably, in the 9-hour follow-up period, high intrinsic autofluorescence in most kidneys
161 interfered with the reliable detection of mCherry fluorescence, limiting the accuracy of
162 direct fluorescence measurements. To overcome this, immunohistochemistry was
163 employed to visualize mCherry localization at the cellular level. This showed broad
164 expression across the tissue, including expression within both glomerular and tubular
165 structures (Figure 5a). BRISH analysis detecting mCherry mRNA confirmed the widespread
166 tissue distribution of mCherry mRNA, highlighting the effective tissue penetration of LNPs
167 after the *ex vivo* intra-arterial administration (Figure 5b). The mRNA signal was
168 predominantly detected intracellularly within the endothelium, although it was also
169 observed in other renal cell types (Figure 5b).
170
171 **Translational studies in human kidneys**
172 Next, the feasibility of mRNA therapy in human deceased donor kidneys was investigated
173 (see Supplemental Table 2 for donor characteristics). DSPE- and TPGS-LNPs carrying
174 mCherry mRNA were administered to 7 human kidneys during NMP using the same
175 protocol as the experiments conducted on porcine kidneys.

176 Within the 12-hour follow-up, mCherry expression was not as abundant compared to the
177 porcine kidneys. Using immunohistochemistry, however, mCherry protein could be
178 detected throughout the tissue of 5 of the treated kidneys, whereas the 2 others failed to
179 induce mCherry expression (Figure 6a). A greater mCherry signal was observed following
180 mRNA delivery via TPGS-LNPs (Figure 6a).
181 BRISH analysis confirmed that both DSPE- and TPGS-LNPs achieved intracellular mRNA
182 delivery throughout the human kidneys (Figure 6b), consistent with the findings in porcine
183 kidneys.
184 Similarly to the porcine kidneys, perfusion characteristics including renal blood flow,
185 oxygen consumption and urine production were not statistically affected by the LNP-
186 mRNA infusion in the human deceased donor kidneys (supplemental Figure 6).
187

188 **DISCUSSION**

189 This study establishes a clinically compatible strategy for organ-directed mRNA delivery
190 during *ex vivo* perfusion. By delivering the mRNA to the isolated organ, off-target effects
191 commonly associated with systemic mRNA delivery are minimized, including hepatic
192 interactions (9). Intra-vascular LNP administration via the renal artery achieved effective
193 tissue penetration and biodistribution of the reporter mRNAs. hEPO expression became
194 detectable around 2 hours after mRNA administration, reaching biologically relevant levels
195 during NMP. The rapid appearance of the mRNA ensures the presence of the encoded
196 proteins during the critical post-transplant period, potentially driving new therapeutic

197 strategies to mitigate IRI, promote tissue regeneration, and ultimately improve organ
198 transplantation outcomes.
199 Building upon previously validated ionizable lipid-based LNP formulations(14), we utilized
200 three different PEG-lipids: Pluronic F127, TPGS, and DSPE-PEG2000, each contributing
201 unique properties (15-18). While all formulations showed comparable physical
202 characteristics, DSPE-PEG2000 and F127 achieved slightly higher mRNA encapsulation
203 efficiencies than TPGS. This may relate to TPGS's smaller lipid head group and shorter PEG
204 chain, potentially compromising particle stability.
205 Our results indicate that when delivering mRNA to whole porcine and human kidneys *ex*
206 *vivo*, LNPs containing TPGS as the PEG-lipid achieved markedly higher protein expression
207 compared to the conventional DSPE-PEG2000. This correlates with the *in vitro* findings,
208 where TPGS-LNP outperformed the other formulations in terms of expression of the
209 reporter protein. The enhanced potency of TPGS-containing LNPs under *ex vivo* conditions
210 may be partly explained by the ability of TPGS to inhibit P-glycoprotein activity(16, 19, 20)
211 which is highly expressed in proximal tubule cells and plays a central role in efflux
212 transport. Beyond serving as a passive stabilizer, TPGS can improve LNP stability within the
213 extracellular milieu, facilitate cellular uptake, and reduce nanoparticle efflux. Moreover, its
214 surfactant-like properties may promote endosomal escape, thereby increasing the
215 probability that delivered mRNA reaches the ribosomal machinery for translation(16).
216 Collectively, these complementary mechanisms could account for the improved
217 biocompatibility, tissue accumulation, and delivery efficiency observed.

218 In our previous *in vivo* work in rodents, mRNA was administered systemically at doses
219 ranging from 0.01 to 1 mg mRNA/kg (22-24). Based on these studies a dose of 0.15 mg
220 mRNA encapsulated in 1 mg of LNPs was selected per porcine or human kidney(21-23). In
221 comparison, a clinical trial investigating VEGF mRNA delivery via epicardial injection used
222 a total dose of 3 mg mRNA(24). Another study investigating an mRNA-based replacement
223 therapy for cystic fibrosis utilized CO-hCFTR mRNA via nebulizer, with nominal doses
224 ranging between 4-24 mg mRNA(5). Notably, the relatively low dose of 0.15 mg mRNA per
225 porcine kidney (weighing approximately 100–150 g) used in our study resulted in high levels
226 of human EPO reaching up to 400 mIU/mL in the perfusate. For comparison, normal
227 circulating EPO concentrations in healthy individuals range from 2.8 to 17.1 mIU/mL(25).
228 In the present study, kidney-NMP was used as a delivery platform and perfusion time was
229 extended to monitor therapeutic protein expression for up to 12 hours. Using mRNA
230 therapeutics, *in vitro* systems have demonstrated sustained protein expression for up to a
231 few days(26, 27), while *in vivo*, systemic peak expression typically occurs at 6 hours and
232 then decreases(28, 29). A transient expression of therapeutic proteins without long-term
233 effects is particularly advantageous for targeting the pathogenic pathways following IRI,
234 observed directly in the period after organ transplantation(30-32).

235 *Ex vivo* mRNA delivery was successfully achieved using human-sized porcine kidneys or
236 human donor kidneys using a clinically compatible NMP setup, identical to those
237 employed in clinical studies(33, 34). Furthermore, LNPs were administered through a
238 simple infusion via the arterial port of the NMP setup, confirming the clinical feasibility of
239 the approach. The lower mCherry protein expression observed in the human kidneys may

240 reflect their larger organ size and variable donor-related factors, including age and
241 comorbidity, duration of warm ischemia during procurement surgery and cold storage,
242 potentially necessitating higher doses.

243 LNP-mRNA treatment was well tolerated during NMP, with preserved perfusion parameters
244 and renal architecture. Additionally, no evidence of cytotoxicity was detected *in vitro* or
245 observed *ex vivo*. Adverse effects seen in systemically delivered LNP-mRNA studies are not
246 anticipated in our ex vivo approach, as systemic exposure is minimized. Moreover,
247 following NMP, it is standard clinical procedure to flush the kidney and/or return it to HMP
248 prior to transplantation, which facilitates the removal of any free LNPs.

249 Given the complex and multifactorial nature of IRI, it may be necessary to target multiple
250 pathways(35). Donor kidneys would greatly benefit from a combined and individualized
251 treatment strategy and mRNA therapy offers a flexible platform for such an approach, as it
252 can encode both gain-of-function activators and inhibitors, which could potentially be
253 combined into a single solution. The rapid protein expression following *ex vivo* delivery of
254 mRNA therapeutics enables the use of these therapeutics to transiently modify the donor
255 organ during preservation, enhancing graft resilience during the critical period immediately
256 following transplantation(31, 32, 35).

257 In summary, we have successfully developed and screened LNPs for efficient mRNA
258 delivery to the kidney during NMP. TPGS-based LNPs emerged as a promising vector for
259 mRNA therapeutics to an isolated kidney, demonstrating their efficacy both *in vitro* and *ex*
260 *vivo* in porcine and human kidneys. Furthermore, we established a practical strategy for

261 using mRNA therapeutics in donor organs, providing a foundation for their application in *ex*
262 *vivo* normothermic machine perfusion as a precision medicine platform prior to organ
263 transplantation.

264 **MATERIALS AND METHODS**

265 **Cell culture**

266 Opossum kidney cells (OK cells) were cultured in low glucose Dulbecco's Modified Eagle
267 Medium (DMEM) (Thermo Fisher, Waltham, MA), supplemented with 10% fetal bovine
268 serum (FBS, Thermo Fisher, Waltham, MA) and 1% penicillin-streptomycin (Thermo Fisher,
269 Waltham, MA) at 37°C, 5% CO_2 and 100% humidity.
270

271 **Preparation of nanoparticles**

272 Lipid nanoparticles (LNP) were synthesized through nanoprecipitation. Briefly, Pluronic
273 (F127, Sigma-Aldrich), C14120(36), cholesterol (Sigma-Aldrich), 1,2-dioleoyl-sn-glycero-3-
274 phosphocholine (DOPC, Avanti Polar Lipids) and d-α-tocopheryl polyethyleneglycol 1000
275 succinate (TPGS, Sigma-Aldrich) were dissolved in 100% ethanol. For F127-LNP, F127 and
276 C14120 were combined at the weight ratio of 2:1. For DSPE-LNP and TPGS-LNP, C14120,
277 cholesterol, DOPC, and the PEG-Lipid either TPGS or 2-distearoyl-sn-glycero-3-
278 phosphoethanolamine-N-[methoxy(polyethylene glycol)-2000] (DSPE-PEG2000, Avanti
279 Polar Lipids) were combined at weight ratio of 4:2:1:1. Subsequently, sodium acetate
280 (200mM, pH 5.5) was rapidly injected into the organic lipid mixture with vigorous stirring,
281 leading to be self-assembly of empty nanoparticles. Ethanol was removed by dialysis

282 against 200 mM sodium acetate pH 5.5 using a 3.5 kDa dialysis tube (Thermo Scientific).

283 LNPs were stored at 4°C and used within one month.

284

285 **mRNA encapsulation and delivery**

286 The following mRNAs were used: CleanCap EPO mRNA (5moU, Trilink, L-7209), CleanCap

287 mCherry mRNA (5moU, Trilink, L-7203) and CleanCap Cy5 eGFP mRNA (5 moU, Trilink, L-

288 7701). mRNA was encapsulated through electrostatic interaction when thoroughly mixed

289 with the LNPs.

290 For in vitro studies, LNPs (1 mg/mL, concentration of C14120) in 200 mM sodium acetate

291 buffer pH 5.5) were mixed with mRNA (at 200 ng/µL) at different N/P ratios. 100 ng of mRNA

292 was mixed with 0.75 µL, 1.5 µL, and 2 µL of LNPs to obtain N/P ratios of 6, 12 and 16,

293 respectively. The LNP/mRNA mixture was incubated for 10 minutes at room temperature

294 (RT) and added to the culture medium.

295 For delivery during kidney NMP, 1100 µg LNPs (in 2.5 mL 200 mM acetate buffer, pH 5.5)

296 were mixed with 150 µg of mRNA (prediluted in 0.5 mL of nuclease-free water) and

297 incubated for 10 minutes at RT. Prior to the infusion, 2 mL of isotonic saline (0.9 mg/mL

298 NaCl Fresenius Kabi, B05BB01) was added. This solution was transferred to a 20 mL

299 syringe and administered via the arterial side of the NMP circuit at an infusion rate of 120

300 mL/h, starting 30 minutes after the initiation of kidney-NMP. Following the initial infusion,

301 the line was flushed with 3 mL of isotonic saline.

302

303 **Characterization of LNPs**

304 The hydrodynamic diameter and surface charge of the LNPs were determined by photon
305 correlation spectroscopy (PCS) and Laser Doppler Velocimetry (LDV) at 25 °C on a
306 Zetasizer Nano ZS (Malvern Instruments, Malvern, UK). The encapsulation efficiency of
307 mRNA was quantified using the RiboGreen assay (Invitrogen, Copenhagen) following the
308 manufacturer's protocol. Briefly, 50 µL of LNP/mRNA solution was mixed with 50 µL of
309 RiboGreen working solution (1:100 in TE buffer: 10 mM Tris, 0.1 mM EDTA, pH 7.5). After 5
310 minutes of incubation at RT, the fluorescence intensity was measured by FLUOstar
311 OPTIMA (Moritex BioSience) at an excitation/emission wavelength of 480/520 nm.
312
313 **Cell viability test**
314 Cell viability was evaluated via AlarmaBlue (Molecular Probes, Life Technologies) assay
315 according to the instructions from the manufacturer. OK cells were seeded in a 96-well
316 plate at a density of $1x10^4$ cells/well. The following day, the growth medium was refreshed
317 and each well was transfected with 33 ng LNP-encapsulated mCherry mRNA. After 24
318 hours, growth medium supplemented with 10% (v/v) of AlarmaBlue reagent was added.
319 After 2 hours of incubation, 80 µL of the supernatant was transferred to an opaque 96-well
320 NUNC plate (Sigma-Aldrich, P8616), and the fluorescence intensity was measured using a
321 FLUOstar OPTIMA plate reader (Moritex BioScience) at excitation and emission
322 wavelengths of 540 nm and 590 nm, respectively.
323
324 **Stability of mRNA encapsulated in LNPs**

325 To assess stability, 88 ng of LNP-encapsulated mCherry mRNA was incubated in 45 μL of
326 NMP perfusate (see supplemental table 1) at 37°C for 0 minutes (right after mixing), 15
327 minutes, 30 minutes, 1 hour, 2 hours, 4 hours, 6 hours and 24 hours. After incubation, lysis
328 buffer (0.25% Igepal CA-630, 10mM Tris·HCl pH 7.4, 150 mM NaCl, and 1 U/μL RNase
329 inhibitor) was added and samples were centrifuged at 10,000 g for 5 minutes. Next, 10 μL
330 of supernatant was used directly for cDNA preparation using Revert Aid RT Reverse
331 Transcription Kit (Thermo Fisher). The cDNA was diluted 40 times, and 4 μL was used as
332 template for quantitative real-time PCR using SYBR Green Master Mix (Thermo Fisher),
333 running on a Light Cycler 480 Real-Time PCR System (Roche). The primer sequences for
334 mCherry are: Forward 5'-CGGGTGATGAACTTCGAGGA-3' and Reverse 5'-
335 TCGAAGTTCATCACCCGCTC-3'.
336
337 **In vitro performance of LNPs for mRNA delivery**
338 OK cells were seeded in 24-well plate ($1x10^5$ cells/well). The next day, growth medium was
339 refreshed and 200 ng LNP-encapsulated mRNA was added per well. After 24 hours, cells
340 were detached using 0.05% Trypsin-EDTA (Thermo Fisher, Waltham, MA) and fluorescent
341 intensity was quantified by flow cytometry (NovoCyte, ACEA Biosciences).
342 For microscopy studies, OK cells were seeded in 8-well μ-Slide (ibiTreat, ibidi; $5x10^4$
343 cells/well). The next day, the growth medium was refreshed and 100 ng LNP-encapsulated
344 mRNA was added per well. After 24 hours, medium was replaced by FluoroBrite DMEM
345 (Thermo Fisher Scientific, Waltham, MA), and cells were imaged by confocal laser

346 scanning microscopy (LSM 710, Zeiss, Germany) and analyzed by Fiji ImageJ software
347 2.3.0.
348
349 **Organ procurement and normothermic machine perfusion**
350 A comprehensive account of the ethical approval process, surgical techniques and blood
351 processing procedures is available in Supplemental Material 1.
352 Porcine kidneys were procured under general anesthesia following a standardized surgical
353 protocol, including midline laparotomy and bilateral nephrectomy with a warm ischemia
354 time as in a living donation procedure. Special care was taken to preserve vascular
355 integrity and obtain sufficient arterial length for optimal cannulation. The renal artery was
356 cannulated with a straight t-cannula immediately post-nephrectomy and with minimal
357 warm ischemic time. Then, the kidney was flushed with heparinized saline followed by cold
358 preservation solution before being stored at 4 ºC. Human kidneys, procured initially with
359 the intent for transplantation but later declined, were transported on hypothermic machine
360 perfusion and re-cannulated upon arrival using appropriately sized arterial and ureteral
361 cannulas. Further procedural details are provided in the Supplemental Material 1.
362 After a maximum of 32 hours of cold ischemia, all kidneys were connected to an open
363 clinically compatible NMP system via the arterial cannula and venous outflow drained
364 freely into the reservoir under gravity, permitted via an uncannulated renal vein.
365 The NMP circuit was primed with 600 mL human albumin erythrocyte-based solution (see
366 composition supplemental material 2). The perfusate temperature was kept at 37ºC and
367 oxygenated with 0.5 L/minute carbogen gas (95% O2, 5% CO2). After the kidney was

368 connected to the system, a mean arterial pressure of 80 mmHg was maintained. Gas
369 analysis was carried out every hour (ABL90 FLEX, Radiometer) and hourly perfusate, urine
370 and biopsies were taken. Urine output was measured, and the rest of the urine was
371 recirculated. During NMP, glucose and pH were adjusted if glucose dropped under 5 mmol
372 and pH under 7.35 by adding a bolus of glucose 5% (50 mg/mL, Fresenius Kabi,
373 7340022100429) or sodium bicarbonate 8.4% (8.4 g/mL, Fresenius Kabi, 03058282)
374 directly to the organ chamber.
375
376 **Sampling and storage**
377 During follow-up on NMP, perfusate from the vein and urine samples were collected.
378 Samples were centrifuged for 12 minutes at 3000 g at 4°C and supernatant was stored at -
379 80°C. Blood gases from arterial and venous perfusate as well as urine, were measured
380 hourly (ABL90 FLEX, Radiometer) to monitor the perfusion process. Each 6 mm biopsy was
381 stored in RNA-later (Merck KGaA) at -80°C. At the end of the perfusion 1x1 cm biopsies with
382 both cortex and medulla were taken and formalin fixed (Biopsafe, 3178-200-03) for about
383 24 hours at 4°C, and were then changed to phosphate buffered saline until embedding.
384
385 **Human EPO ELISA**
386 Human EPO protein expression in kidney NMP perfusate and urine samples was quantified
387 by a Human EPO ELISA (Invitrogen, BMS2035-2). Human EPO in OK cell cultures was
388 quantified by an EPO DuoSet ELISA (R&D Systems, DY286-05) according to the
389 manufacturer's protocols.

390 **mCherry Western Blot**

391 In total, 25 mg of kidney tissue was homogenized in M tubes (Miltenyi Biotec,130093236) in
392 500 µL of Pierce RIPA buffer (Thermo Scientific, 89901) supplemented with cOmplete Mini
393 protease inhibitor cocktail (Merck KGaA, 11836153001). Lysates were centrifuged (10
394 minutes, 3000 g, 4°C) and supernatant was stored at -80ºC until further use. Total protein
395 was quantified using Pierce BCA Protein Assay Kit (Thermo Fisher, 23225) according to the
396 manufacturer's protocols. In total, 30 µg of protein was run on an Any kD CriterionTM TGX
397 Stain-Free gel (BIO-RAD, 5678124) and transferred onto nitrocellulose Trans-Blot®TurboTM
398 membranes (BIO-RAD, 1704159). Blots were blocked using 5% Skim milk powder
399 (Millipore, 999999-99-4) and washed in 20 mM TBS-T (Tris-buffered saline, pH 7.6, 0.1%
400 TWEEN 20). Membranes were incubated with 0.35 µg/ml DSHB-mCherry-3A11-s antibody
401 (Development Studies Hybridoma Bank, DSHB) in 20 mL of TBS-T overnight at 4°C,
402 followed by 1 hour of incubation at RT. After being washed in TBS-T, blots were incubated
403 with 0.4 µg/ml polyclonal Goat Anti-mouse Immunoglobulins/HRP antibody (Aligent,
404 P0447) in TBS-T for 1 hour at RT. After wash, blots were incubated with 3 mL ECLTM Prime
405 Western Blotting Detection Reagent (Cytvia, RPN2236) for 5 minutes at RT, and imaged
406 using the ChemiDocTM MP Imaging System (BIO-RAD). Quantification of bands in the blot
407 was done with ImageLab (version 6.0.1, 2017) and signal was corrected for total protein of
408 the respective gel.

409

410 **Immunofluorescence (IF) and microscopy**

411 The formalin-fixed paraffin-embedded (FFPE) samples were sectioned at 2.5 µm with a
412 microtome (Thermo Scientific, HM3555). Hematoxylin and eosin (H&E) and Periodic Acid–
413 Schiff (PAS) staining were performed on FFPE kidney sections (3–4 µm thick) using
414 standard protocols. H&E was used to evaluate general tissue morphology, while PAS
415 staining was used to assess glomerular basement membranes, tubular brush borders, and
416 mesangial matrix integrity. Histological scoring was performed by a trained pathologist
417 blinded to the treatment groups. Kidney sections were evaluated for features including
418 tubular damage, dilatation, cast formation, vacuolization, glomerular injury, interstitial
419 inflammation, and edema. Each parameter was semi-quantitatively scored based on
420 predefined criteria, and overall tissue integrity was assessed to compare damage and
421 structural preservation between groups.
422 Before IF staining, kidney FFPE samples were heated at 60°C and deparaffinized with
423 xylene (BDH Chemicals, 28973-363). Antigen retrieval was performed by immersing the
424 slides in a preheated antigen retrieval buffer (1.21 g Tris (Sigma T-1378), 0.19 g EGTA
425 (Triplex VI, Merck 8435) in 1L of MilliQ water, pH 9.0) and heating them at 95-100°C for 10-
426 20 minutes. After, the sections were allowed to cool down for about 20 minutes at RT.
427 Then, the sections were washed and permeabilized in TBS-T for 10 minutes at RT. Sections
428 were placed at RT for 10 minutes then fixed with 4% paraformaldehyde (PFA) for 15
429 minutes. Following a 5-minute wash with TBS (Tris-NaCl buffered saline, 20 mM Tris, 150
430 mM NaCl, pH 7.2) the sections were blocked for 1 hour at RT using horse serum (5% for
431 human kidneys and 1% for porcine kidneys, Thermo Fisher, 26050088) in TBS-T (0.2%
432 Triton X100 in TBS). Next, the sections were incubated for 2 hours with 2 µg/mL DSHB-

433 mCherry-3A11-s antibody in TBS-T supplemented with 2.5% horse serum for human
434 kidneys and 0.5% horse serum for porcine kidneys. After three 10-minute washes with TBS,
435 the sections were incubated with 5 µg/mL Polyclonal Goat Anti-Mouse
436 Immunoglobulins/CF647 antibody (Sigma Aldrich, SAB4600182) in TBS-T, for 1 hour at RT.
437 This was followed by another three 5-minute washes with TBS. Finally, the sections were
438 mounted with ProLong Diamond Antifade Mountant with 4',6-diamidino-2-phenylindole
439 (DAPI) mounting media (Thermo Fisher Scientific, P36962) and stored at 4°C until
440 observation with confocal microscopy (LSM 800 Airyscan, Zeiss) and VS120 Slides Scanner
441 (Olympus). The images obtained were processed using either Fiji (version 1) or Qu Path
442 (version 0.5.1-arm64) software.
443
444 **Brightfield RNA In Situ Hybridization (BRISH)**
445 RNA-ISH was performed by using the RNAscope Probe-mCherry-O10-C1 (Cat. No.
446 1264111-C1, target region 2-714 bp), which is a probe specific mCherry mRNA. For RNA
447 quality controls, probes targeting the housekeeping gene peptidylprolyl isomerase B
448 (cyclophilin B) were used as follows: Ss-PPIB (Cat. No. 428591, target region 16-642 bp) for
449 pig tissue, and Hs-PPIB (Cat. No. probe. 313901, target region 139-989 bp) for human
450 tissue and cells.
451 As specificity control for mCherry detection, about 100.000 HEK293 cells were transfected
452 with 200 ng mCherry mRNA carried by 1.5 µg of TPGS-LNP for 24 hours. HEK293 cells
453 incubated for 24 hours without transfection were used as controls. Cells were fixed with
454 4% paraformaldehyde (PFA) for 1 hour and placed in agar solution (0.18 g of agar in 10 mL

455 of demineralized water). Followed by a second fixation with 4% PFA and paraffin
456 embedding.
457 RNA-BRISH was performed on 5-µm-thick FFPE sections on SuperFrost PLUS microscope
458 slides. Pretreatment was done following the RNAscope Sample Preparation and
459 Pretreatment Guide for FFPE Tissue (Cat. No. 322381). This included blocking H_2O_2 by
460 adding the RNAscope hydrogen peroxide to the slides and incubating them for 10 minutes
461 at RT. Antigen retrieval was performed by heating the slides for 18 minutes in the
462 RNAscope antigen retrieval buffer (1:10 dilution and 98-100 °C) using a steamer. Then,
463 protease treatment was performed by adding the RNAscope Protease Plus to the sections
464 and incubating them at 40°C for 30 minutes in the HybEZ oven, followed by probe
465 hybridization overnight. Signals were detected by using the RNAscope 2.0 HD Detection Kit
466 (Cat. No. 322310). This included amplification by a series of amplification steps and signal
467 detection by using DAB (3,3'-Diaminobenzidine). The reactivity was visualized as brown
468 dots. Following BRISH, nuclear counterstaining was performed using hematoxylin.
469 Sections were coverslipped and digitized using an Olympus SLIDEVIEW VS200 slide
470 scanner (Olympus Nederland B.V., Hoofddorp, Netherlands).
471
472 **Data analysis**
473 GraphPad Prism (version 10.2.2) was used to perform statistical analyses and compose
474 graphs. Data are presented as mean ± SD unless otherwise stated. Statistical tests
475 included two-way ANOVA, t-tests, and appropriate non-parametric tests based on data
476 distribution. Statistical significance was set to $p < 0.05$.

DATA AVAILABILITY STATEMENT

Raw numerical data underlying Figures 1–4 and Supplementary Figures S1–S4 (GraphPad Prism files) are available upon request.

ACKNOWLEDGEMENTS

The authors would like to express their gratitude to the 34Lives team, especially, Kathleen St Jean, Stephen Eilert, Haley Frost and Ali Smith, for hosting the translational experiments providing the opportunity to perform studies with human deceased donor kidneys and arranging the logistics for transport and infrastructure. This study would not have been possible without the gracious gifts from the generous donor families and through collaborations with Kentucky Organ Donor Affiliates (Network for Hope), Life Connection of Ohio, Gift of Hope, Texas Organ Sharing Alliance, LifeGift, Indiana Donor Network, Iowa Donor Network, and Lifeline of Ohio. We acknowledge Mirjiam Mastik for her valuable assistance in carrying out the BRISH studies. Fluorescent Microscopy experiments were supported by the Scientific Service Units (SSU) of Institute of Science and Technology (ISTA) through resources provided from the Imaging and Optics Facility (IOF), and personal support of Josephine Pfiefer and Bernhard Hochreiter. Scoring of kidney tissue sections was supported by pathologist Søren Rasmus Palmelund Krag. And lastly, the authors would like to acknowledge Lene Mejer Rosenlund, Maria Arge and Birgitte Kildevæd Sahl for their expert biotechnician assitance. This work was supported by Augustinus Fonden and Novo Nordisk Foundation grant NNF23OC0081177 (RNA-META).

521 **AUTHOR CONTRIBUTIONS**

522 ME, JK, BJ, AK, RN, HL, CBB and PS conceptualized the research design. CBB, PS, KBK,
523 VRL, CJ and AVF participated in the performance of the experiments. CBB, PS and JH
524 participated in the analysis. CBB and PS drafted the manuscript. ME performed critical
525 revision. ME, JK, BJ and AK supervised the project and reviewed the final version of this
526 manuscript. All authors approved the final version of the manuscript.

527

528

529

530

531

532

533

534

535

536

537

538

539

540

541

542

DECLARATION OF INTERESTS

There are no conflicts of interest.

KEY WORDS

mRNA therapeutics, , donor organs, kidney machine perfusion, graft optimization, LNPs

587 **REFERENCES**

588 1. Walsh EE, Frenck RW, Jr., Falsey AR, Kitchin N, Absalon J, Gurtman A, et al. Safety
589 and Immunogenicity of Two RNA-Based Covid-19 Vaccine Candidates. N Engl J Med.
590 2020;383(25):2439-50.
591 2. Baden LR, El Sahly HM, Essink B, Kotloff K, Frey S, Novak R, et al. Efficacy and Safety
592 of the mRNA-1273 SARS-CoV-2 Vaccine. N Engl J Med. 2021;384(5):403-16.
593 3. Sahin U, Oehm P, Derhovanessian E, Jabulowsky RA, Vormehr M, Gold M, et al. An
594 RNA vaccine drives immunity in checkpoint-inhibitor-treated melanoma. Nature.
595 2020;585(7823):107-12.
596 4. Parhiz H, Atochina-Vasserman EN, Weissman D. mRNA-based therapeutics:
597 looking beyond COVID-19 vaccines. Lancet. 2024;403(10432):1192-204.
598 5. Rowe SM, Zuckerman JB, Dorgan D, Lascano J, McCoy K, Jain M, et al. Inhaled
599 mRNA therapy for treatment of cystic fibrosis: Interim results of a randomized, double-
600 blind, placebo-controlled phase 1/2 clinical study. J Cyst Fibros. 2023;22(4):656-64.
601 6. Anttila V, Saraste A, Knuuti J, Jaakkola P, Hedman M, Svedlund S, et al. Synthetic
602 mRNA Encoding VEGF-A in Patients Undergoing Coronary Artery Bypass Grafting: Design of
603 a Phase 2a Clinical Trial. Mol Ther Methods Clin Dev. 2020;18:464-72.
604 7. Hou X, Zaks T, Langer R, Dong Y. Lipid nanoparticles for mRNA delivery. Nat Rev
605 Mater. 2021;6(12):1078-94.
606 8. Whitehead KA, Langer R, Anderson DG. Knocking down barriers: advances in siRNA
607 delivery. Nat Rev Drug Discov. 2009;8(2):129-38.
608 9. Sebastiani F, Yanez Arteta M, Lerche M, Porcar L, Lang C, Bragg RA, et al.
609 Apolipoprotein E Binding Drives Structural and Compositional Rearrangement of mRNA-
610 Containing Lipid Nanoparticles. ACS Nano. 2021;15(4):6709-22.
611 10. Moers C, Smits JM, Maathuis MH, Treckmann J, van Gelder F, Napieralski BP, et al.
612 Machine perfusion or cold storage in deceased-donor kidney transplantation. N Engl J
613 Med. 2009;360(1):7-19.
614 11. Ceresa CDL, Nasralla D, Pollok JM, Friend PJ. Machine perfusion of the liver:
615 applications in transplantation and beyond. Nat Rev Gastroenterol Hepatol.
616 2022;19(3):199-209.
617 12. Rega F, Lebreton G, Para M, Michel S, Schramm R, Begot E, et al. Hypothermic
618 oxygenated perfusion of the donor heart in heart transplantation: the short-term outcome
619 from a randomised, controlled, open-label, multicentre clinical trial. Lancet.
620 2024;404(10453):670-82.
621 13. Lasorsa F, Rutigliano M, Milella M, d'Amati A, Crocetto F, Pandolfo SD, et al.
622 Ischemia-Reperfusion Injury in Kidney Transplantation: Mechanisms and Potential
623 Therapeutic Targets. Int J Mol Sci. 2024;25(8).
624 14. Song P, Yang C, Thomsen JS, Dagnaes-Hansen F, Jakobsen M, Bruel A, et al.
625 Lipidoid-siRNA Nanoparticle-Mediated IL-1beta Gene Silencing for Systemic Arthritis
626 Therapy in a Mouse Model. Mol Ther. 2019;27(8):1424-35.
627 15. Hald Albertsen C, Kulkarni JA, Witzigmann D, Lind M, Petersson K, Simonsen JB. The
628 role of lipid components in lipid nanoparticles for vaccines and gene therapy. Adv Drug
629 Deliv Rev. 2022;188:114416.

630 16. Yang C, Wu T, Qi Y, Zhang Z. Recent Advances in the Application of Vitamin E TPGS
631 for Drug Delivery. Theranostics. 2018;8(2):464-85.
632 17. Yu H, Dyett BP, Zhai J, Strachan JB, Drummond CJ, Conn CE. Formation of
633 particulate lipid lyotropic liquid crystalline nanocarriers using a microfluidic platform. J
634 Colloid Interface Sci. 2023;634:279-89.
635 18. Akash MS, Rehman K. Recent progress in biomedical applications of Pluronic
636 (PF127): Pharmaceutical perspectives. J Control Release. 2015;209:120-38.
637 19. Banan Sadeghian R, Ueno R, Takata Y, Kawakami A, Ma C, Araoka T, et al. Cells
638 sorted off hiPSC-derived kidney organoids coupled with immortalized cells reliably model
639 the proximal tubule. Commun Biol. 2023;6(1):483.
640 20. Collnot EM, Baldes C, Wempe MF, Kappl R, Huttermann J, Hyatt JA, et al.
641 Mechanism of inhibition of P-glycoprotein mediated efflux by vitamin E TPGS: influence on
642 ATPase activity and membrane fluidity. Mol Pharm. 2007;4(3):465-74.
643 21. Evers MJW, Du W, Yang Q, Kooijmans SAA, Vink A, van Steenbergen M, et al.
644 Delivery of modified mRNA to damaged myocardium by systemic administration of lipid
645 nanoparticles. J Control Release. 2022;343:207-16.
646 22. Jiang Y, Zhang Y, Liu C, Liu J, Xue W, Wang Z, et al. Tumor-activated IL-2 mRNA
647 delivered by lipid nanoparticles for cancer immunotherapy. J Control Release.
648 2024;368:663-75.
649 23. Zhao S, Gao K, Han H, Stenzel M, Yin B, Song H, et al. Acid-degradable lipid
650 nanoparticles enhance the delivery of mRNA. Nat Nanotechnol. 2024;19(11):1702-11.
651 24. Anttila V, Saraste A, Knuuti J, Hedman M, Jaakkola P, Laugwitz KL, et al. Direct
652 intramyocardial injection of VEGF mRNA in patients undergoing coronary artery bypass
653 grafting. Mol Ther. 2023;31(3):866-74.
654 25. Grote Beverborg N, Verweij N, Klip IT, van der Wal HH, Voors AA, van Veldhuisen DJ,
655 et al. Erythropoietin in the general population: reference ranges and clinical, biochemical
656 and genetic correlates. PLoS One. 2015;10(4):e0125215.
657 26. Liu J, Zhang Y, Liu C, Jiang Y, Wang Z, Guo Z, et al. A single dose of VEGF-A circular
658 RNA sustains in situ long-term expression of protein to accelerate diabetic wound healing.
659 J Control Release. 2024;373:319-35.
660 27. Chen R, Wang SK, Belk JA, Amaya L, Li Z, Cardenas A, et al. Engineering circular RNA
661 for enhanced protein production. Nat Biotechnol. 2023;41(2):262-72.
662 28. Pardi N, Tuyishime S, Muramatsu H, Kariko K, Mui BL, Tam YK, et al. Expression
663 kinetics of nucleoside-modified mRNA delivered in lipid nanoparticles to mice by various
664 routes. J Control Release. 2015;217:345-51.
665 29. Chen H, Liu D, Aditham A, Guo J, Huang J, Kostas F, et al. Chemical and topological
666 design of multicapped mRNA and capped circular RNA to augment translation. Nat
667 Biotechnol. 2024.
668 30. Sharfuddin AA, Molitoris BA. Pathophysiology of ischemic acute kidney injury. Nat
669 Rev Nephrol. 2011;7(4):189-200.
670 31. Legrand M, Mik EG, Johannes T, Payen D, Ince C. Renal hypoxia and dysoxia after
671 reperfusion of the ischemic kidney. Mol Med. 2008;14(7-8):502-16.
672 32. Ponticelli C. Ischaemia-reperfusion injury: a major protagonist in kidney
673 transplantation. Nephrol Dial Transplant. 2014;29(6):1134-40.

674 33. Hosgood SA, Callaghan CJ, Wilson CH, Smith L, Mullings J, Mehew J, et al.
675 Normothermic machine perfusion versus static cold storage in donation after circulatory
676 death kidney transplantation: a randomized controlled trial. Nat Med. 2023;29(6):1511-9.
677 34. An Observational Study of a Dedicated Preservation and Assessment Service to
678 Optimize Organ Utilization for Hard-to-Place Kidneys [Internet]. 2024. Available from:
679 https://clinicaltrials.gov/study/NCT06263023.
680 35. Ogurlu B, Hamelink TL, Van Tricht IM, Leuvenink HGD, De Borst MH, Moers C, et al.
681 Utilizing pathophysiological concepts of ischemia-reperfusion injury to design
682 renoprotective strategies and therapeutic interventions for normothermic ex vivo kidney
683 perfusion. Am J Transplant. 2024;24(7):1110-26.
684 36. Love KT, Mahon KP, Levins CG, Whitehead KA, Querbes W, Dorkin JR, et al. Lipid-
685 like materials for low-dose, in vivo gene silencing. Proc Natl Acad Sci U S A.
686 2010;107(5):1864-9.
687

688

689

690

691

692

693

694

695

696

697

698

699

700

701

702

703 **FIGURE LEGENDS**

704 Figure 1. In vitro Characterization of F127-LNP, TPGS-LNP and DSPE-LNP. (a)
705 Hydrodynamic diameter. (b) Polydispersity index (PDI). (c) Zeta potential. (d) mCherry
706 protein expression and cell viability (e) in OK cells after transfection with LNP-
707 encapsulated mCherry mRNA at N/P ratios of 6,12 and 16. (f) The encapsulation efficiency
708 of F127-LNP, TPGS-LNP and DSPE-LNP at N/P ratio of 12. (g) Stability of free and LNP-
709 encapsulated mCherry mRNA (F127-LNP, TPGS-LNP and DSPE-LNP) in kidney perfusion
710 solution over 24 hours at 37 °C, indicated by ct values measured by RT-qPCR and
711 presented as Mean ± SD (n = 3).

712

713 Figure 2. mRNA uptake and protein expression in OK cells transfected with DSPE-LNP,
714 TPGS-LNP and F127-LNP. (a) Representative confocal images of OK cells transfected with
715 LNP encapsulated with Cy5-labeled eGFP mRNA. Green: eGFP protein expression; red:
716 Cy5-labeled eGFP mRNA (mRNA-Cy5); blue: nucleus stained with Hoechst 33342. (b)
717 Quantitative analysis of cellular uptake of Cy-5 labeled eGFP mRNA and (c) eGFP protein
718 expression. Data are presented as Mean ± SD (n = 3). Statistical significance was
719 determined by multiple mixed effects analysis.* $p < 0.05$, ** $p < 0.01$, *** $p < 0.001$.

720

721 Figure 3: Levels of human erythropoietin (hEPO) detected in perfusate (kidney perfusion
722 solution) and urine following arterial infusion of 150 μg hEPO mRNA via DSPE- and TPGS-
723 LNP during NMP of porcine kidneys. hEPO levels detected by ELISA. (a) Human EPO levels
724 measured in the perfusate over 6 hours. Significance of TPGS-LNP or DSPE-LNP against

725 the control is determined by 2-way ANOVA test with Dunn's multiple comparisons. * $p <$
726 0.05, ** $p < 0.01$, *** $p < 0.001$. (b) Human EPO levels detected in the urine 4-6 hours after
727 mRNA infusion. Significance is determined by Kruskal-Wallis. * $p < 0.05$, ** $p < 0.01$, *** p
728 < 0.001.
729
730 Figure 4: Levels of mCherry detected by western blot throughout several kidney regions
731 following arterial infusion of 150 μg mCherry mRNA via DSPE- and TPGS-LNP during NMP
732 of porcine kidneys. (a) Representative western blot showing mCherry expression (28 kDa)
733 in kidney cortical tissue after delivery with DSPE- and TPGS-LNPs. (b) Bar plot quantifying
734 mCherry levels in different kidney regions, including the cortex (cranial, lateral, caudal)
735 and medulla obtained after the end of the perfusion. Significance is determined by two-
736 way ANOVA and Šídák's multiple comparisons. * $p < 0.05$, ** $p < 0.01$, *** $p < 0.001$.
737
738 Figure 5: mCherry mRNA and mCherry protein presence in kidney tissue following arterial
739 infusion of 150 μg mCherry mRNA via DSPE- and TPGS-LNP during NMP of porcine kidneys.
740 mCherry mRNA presence detected by brightfield microscopy after Brightfield RNA In Situ
741 Hybridation (BRISH) analysis and mCherry protein presence observed by fluorescence
742 microscopy after immunofluorescence (IF). (a) Fluorescence microscopy images of
743 porcine kidney tissue showing mCherry protein expression by IF (red, Alexa 647) and
744 nuclear staining (blue, DAPI) after delivery with DPSE-, TPGS-LNPs and perfused kidneys
745 without mRNA-LNP treatment. (b) Brightfield imaging of BRISH analysis showing the
746 presence of mCherry mRNA (brown precipitate) and hematoxylin counterstaining (blue).

747 Kidney structures are marked accordingly: glomeruli (▲), tubuli (■) and vascular structures

748 (●).

749

750 Figure 6: mCherry mRNA and mCherry protein presence in kidney tissue following arterial

751 infusion of 150 μg mCherry mRNA via DSPE- and TPGS-LNP during NMP of human kidneys.

752 mCherry mRNA presence detected by brightfield microscopy after Brightfield RNA In Situ

753 Hybridation (BRISH) analysis and mCherry protein presence observed by fluorescence

754 microscopy after immunofluorescence (IF). (a) Fluorescence microscopy images of

755 porcine kidney tissue showing mCherry protein expression by IF (red, Alexa 647) and

756 nuclear staining (blue, DAPI) after delivery with DPSE-, TPGS-LNPs and kidneys with no

757 protein expression after mRNA-LNP treatment. (b) Brightfield imaging of BRISH analysis

758 showing the presence of mCherry mRNA (brown precipitate) and hematoxylin

759 counterstaining (blue). Kidney structures are marked accordingly: glomeruli (▲), tubuli (■)

760 and vascular structures (●).

761

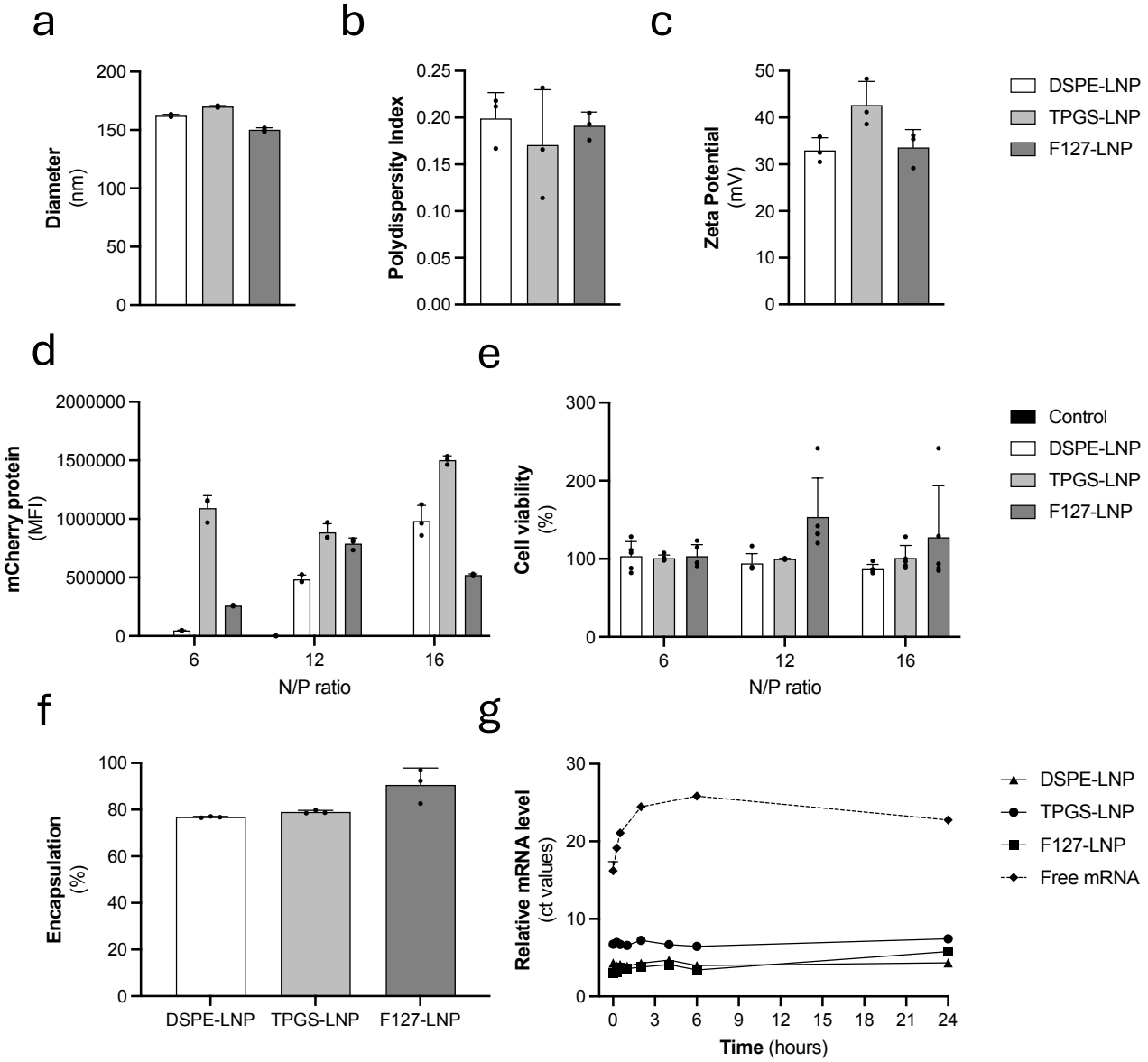
a
Diameter (nm)
200
150
100
50
0
b
Polydispersity Index
0.25
0.20
0.15
0.10
0.05
0.00
c
Zeta Potential (mV)
50
40
30
20
10
0
DSPE-LNP
TPGS-LNP
F127-LNP
d
mCherry protein (MFI)
2000000
1500000
1000000
500000
0
6
12
16
N/P ratio
e
Cell viability (%)
300
200
100
0
6
12
16
N/P ratio
Control
DSPE-LNP
TPGS-LNP
F127-LNP
f
Encapsulation (%)
100
80
60
40
20
0
DSPE-LNP
TPGS-LNP
F127-LNP
g
Relative mRNA level (ct values)
30
20
10
0
0
3
6
9
12
15
18
21
24
Time (hours)
DSPE-LNP
TPGS-LNP
F127-LNP
Free mRNA

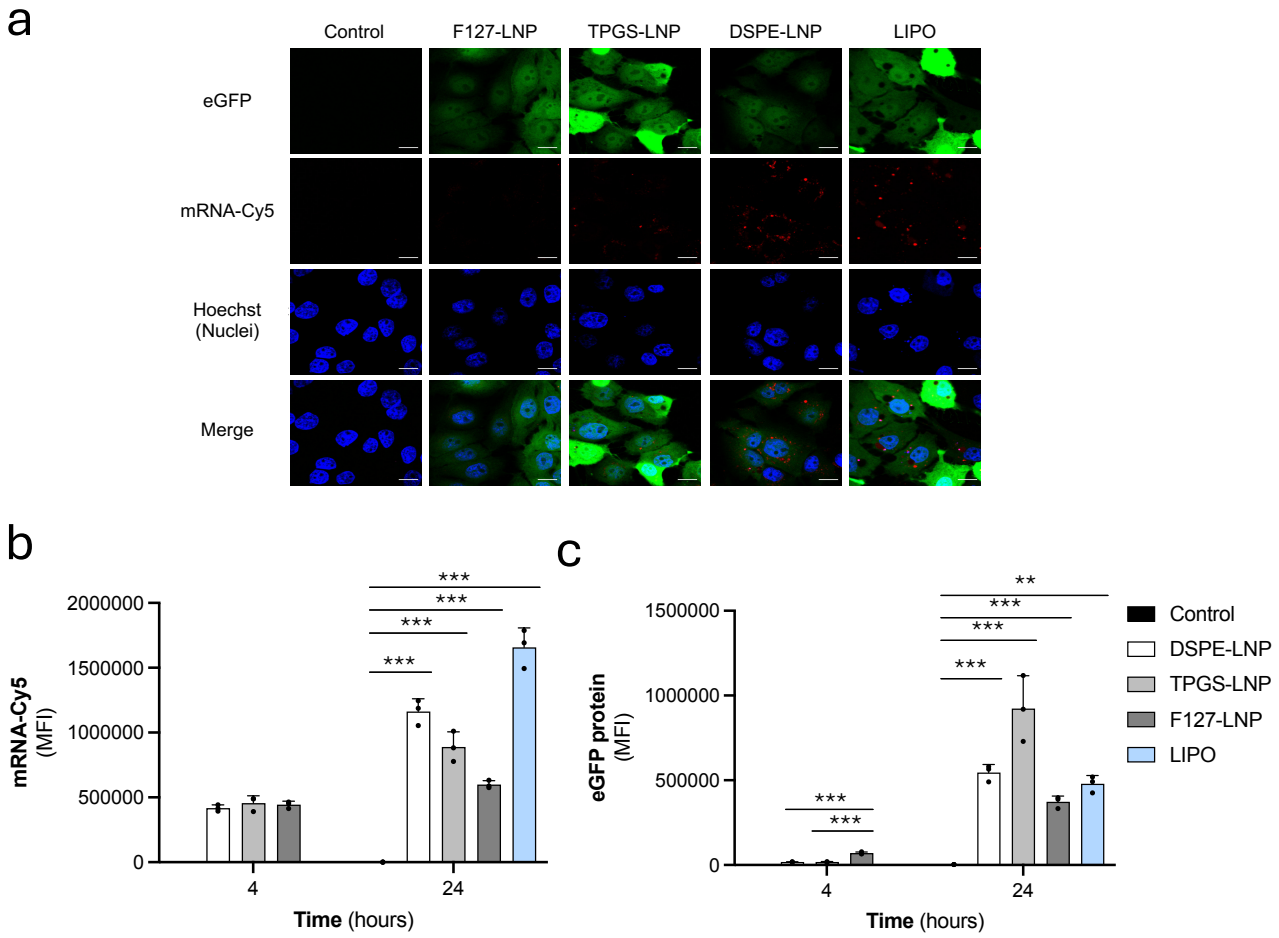
a
Control
F127-LNP
TPGS-LNP
DSPE-LNP
LIPO
eGFP
mRNA-Cy5
Hoechst
(Nuclei)
Merge
b
mRNA-Cy5
(MFI)
2000000
1500000
1000000
500000
0
4
24
Time (hours)
***
c
eGFP protein
(MFI)
1500000
1000000
500000
0
**
Control
DSPE-LNP
TPGS-LNP
F127-LNP
LIPO

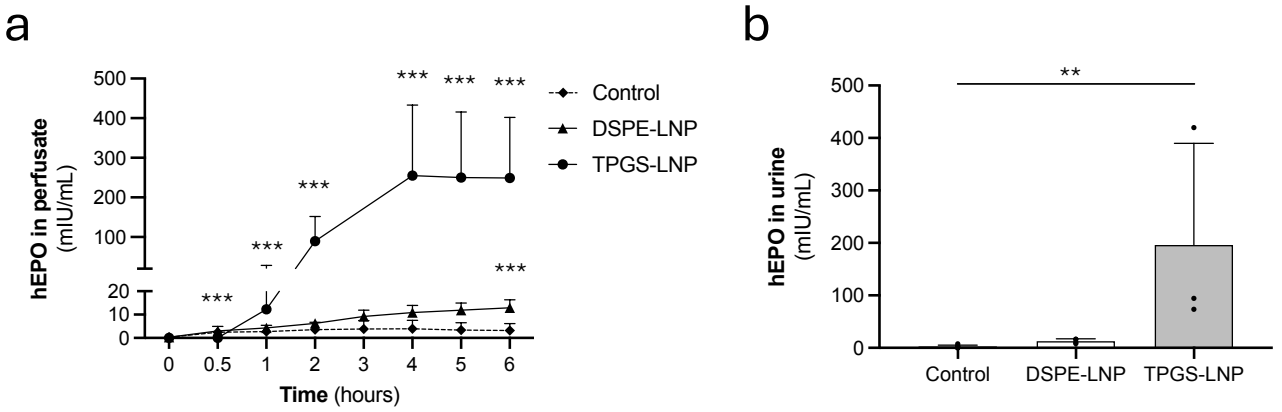
a
hEPO in perfusate
(mIU/mL)
500
400
300
200
100
20
10
0
***
***
***
***
***
***
0
0.5
1
2
3
4
5
6
Time (hours)
Control
DSPE-LNP
TPGS-LNP
b
hEPO in urine
(mIU/mL)
500
400
300
200
100
0
**
Control
DSPE-LNP
TPGS-LNP

a

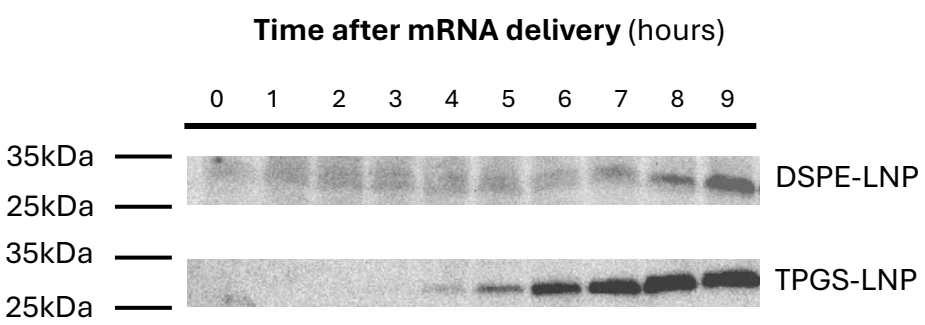
Time after mRNA delivery (hours)
0 1 2 3 4 5 6 7 8 9
35kDa
25kDa
35kDa
25kDa
DSPE-LNP
TPGS-LNP

b

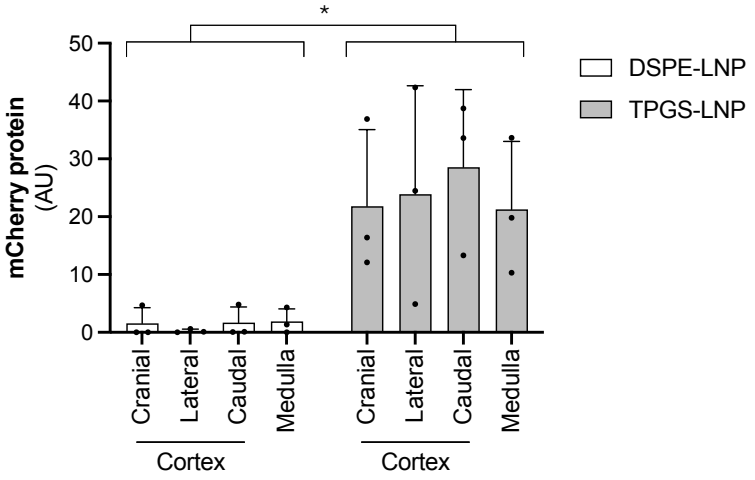
*
mCherry protein (AU)
50
40
30
20
10
0
DSPE-LNP
TPGS-LNP
Cranial
Lateral
Caudal
Medulla
Cranial
Lateral
Caudal
Medulla
Cortex
Cortex

a

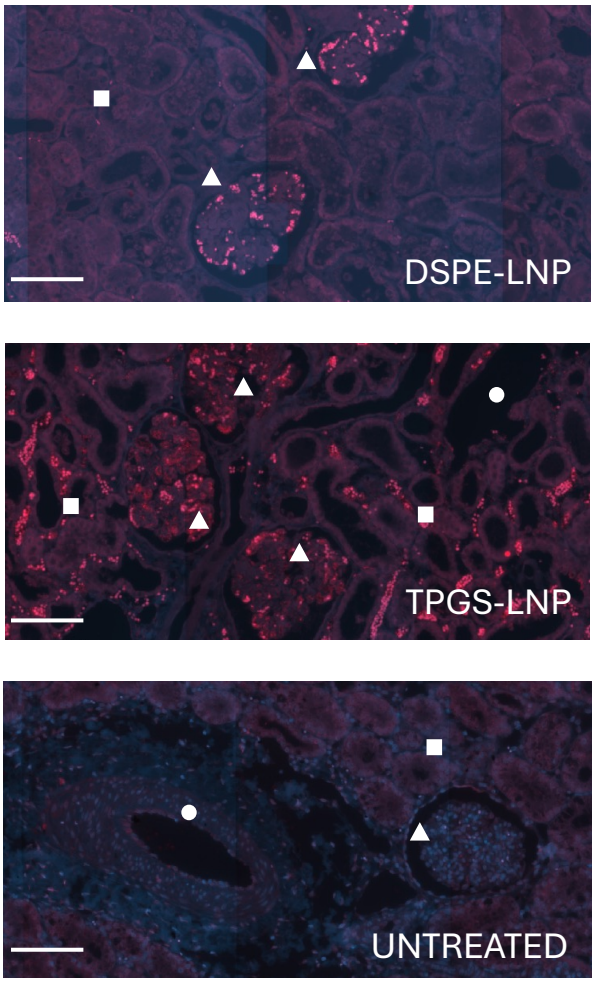

Red: mCherry protein
Blue: DAPI (nuclei)
100 µm

b

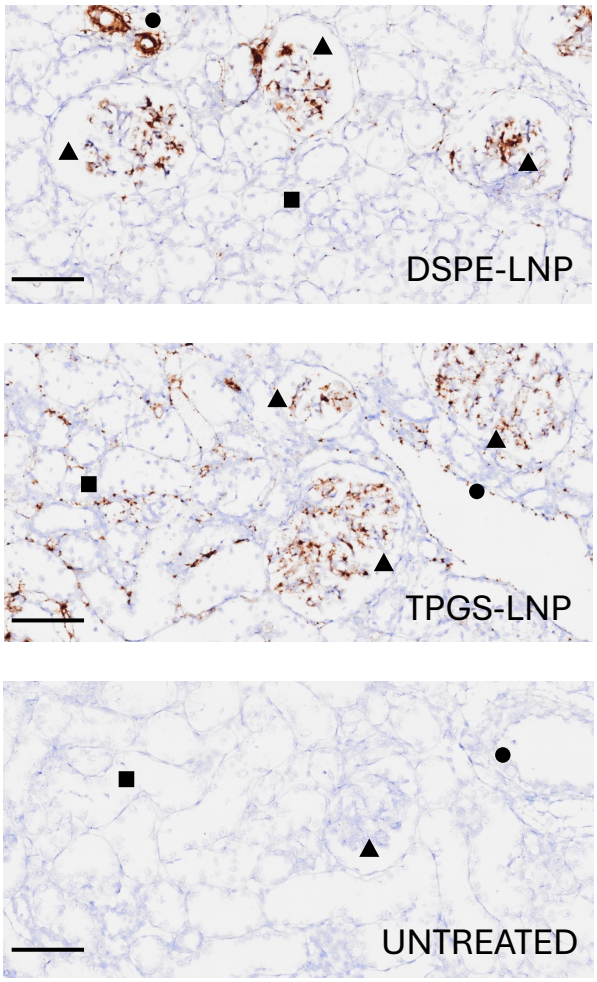

Brown: mCherry mRNA
Blue: Hematoxylin (counterstaining)
100 µm

a

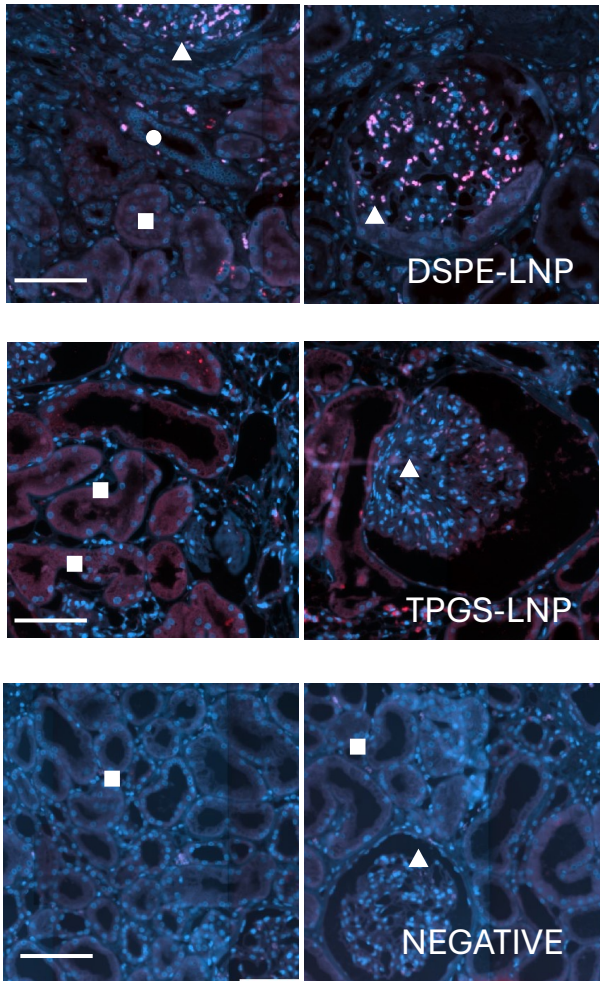

Red: mCherry protein
Blue: DAPI (nuclei)
100 µm

b

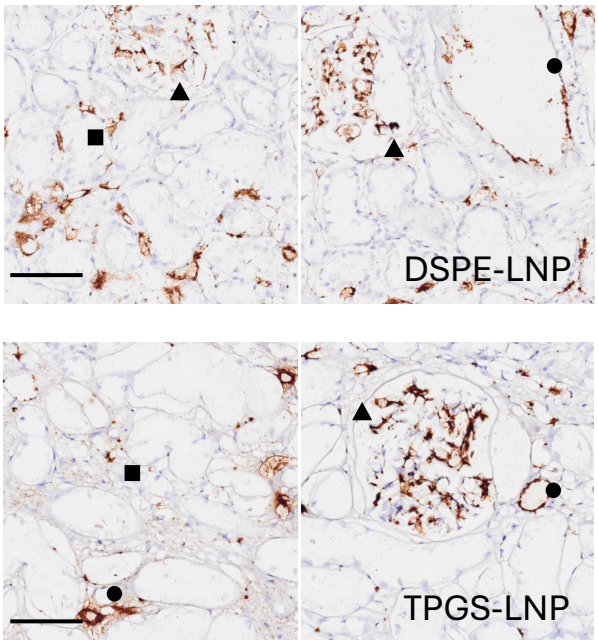

Brown: mCherry mRNA
Blue: Hematoxylin (counterstaining)
100 µm